A thermodynamic approach to *T–P* phase diagrams of substances in liquid and amorphous states

2003 J. Phys.: Condens. Matter 15 6123

(http://iopscience.iop.org/0953-8984/15/36/304)

INSTITUTE OF PHYSICS PUBLISHING JOURNAL OF PHYSICS: CONDENSED MATTER

J. Phys.: Condens. Matter **15** (2003) 6123–6141 PII: S0953-8984(03)55810-6

A thermodynamic approach to T–P phase diagrams of substances in liquid and amorphous states

E G Ponyatovsky

Institute of Solid State Physics, Russian Academy of Sciences, Chernogolovka, Moscow District, 142432, Russia

E-mail: ponyatov@issp.ac.ru

Received 8 November 2002
Published 29 August 2003
Online at stacks.iop.org/JPhysCM/15/6123

Abstract

The metastable phase equilibria of substances in the disordered, liquid or amorphous, state are considered in T–P coordinates. Application of the thermodynamic model of pseudo-binary solutions is illustrated by means of calculated metastable T–P phase diagrams of water, carbon, and semiconducting compounds, GaSb and $Ga_{38}Sb_{38}Ge_{24}$. All calculated diagrams include the equilibrium lines between the disordered phases terminating at the critical points and the stability boundaries of these phases, the spinodals. Depending on the mutual disposition of the elements of the stable and metastable T–P diagrams, two additional lines of metastable equilibria between the crystalline high-pressure phase and each of the metastable disordered phases can appear. These lines terminate at the points of intersection with spinodals. These special points are denoted as pseudo-critical points. A combined analysis of the stable and metastable diagrams gives a reasonable interpretation of the experimental data on the phase transformations and on the nature of the anomalous properties of the substances in question as well as allowing prediction of some new effects.

1. Introduction

The physics of disordered condensed matter, liquid or amorphous, is a subject of increasing research interest at present, as is evidenced also by the contents of this Special Issue. A lot of papers are devoted to the experimental study of the anomalous properties and the phase transitions in liquid and amorphous substances in wide T–P ranges and to the theoretical calculation of the structure and properties of the disordered phases using the molecular dynamics simulation (MDS) methods and the statistical two-level models.

Below, we consider the metastable T–P phase diagrams with first-order transition lines in the regions of the liquid and amorphous phases. The disordered state composed of clusters with essentially different atomic structures is equivalent to multilevel systems as regards their

analytical description. The constitution of such liquid and amorphous phases is a source of many specific features observed over a wide T–P region. The latter include first-order phase transitions terminating at the critical point, thermodynamic instability of the disordered phases at the spinodals, anomalies of the properties in the vicinity of the critical point, as well as the phenomenon of solid-state amorphization (SSA) due to high-pressure treatment. To explain the nature of these phenomena and to quantitatively calculate the anomalies of the thermodynamic properties of the disordered systems, it is necessary to supplement our knowledge of the stable T–P phase diagrams with diagrams of the metastable phase equilibria in these substances. A correlation between the metastable T–P diagrams, the anomalous properties of the disordered phases, and the processes of SSA will be analysed on the basis of the thermodynamic model of the pseudo-binary regular solutions.

2. The model of the pseudo-binary regular solutions

The model is based on the following statements:

(i) Both liquid and amorphous matter consists of clusters whose atomic configurations may already be very different in the first coordination sphere.

(ii) A substance undergoing a first-order transition from a less dense phase to one of higher density, when compressed, consists of two types of cluster. In the ground state at $T = 0$ K, the phase of lower density consists only of clusters with a low coordination number whereas the high-density phase is composed of clusters with a higher coordination number corresponding to the higher density of the substance.

(iii) At $T > 0$ K, both phases consist of clusters of two kinds. These phases are considered as solutions for the corresponding clusters, the clusters being the two components of the solutions.

(iv) The solutions for the clusters are regular. The Gibbs potential of the solutions is of the form

$$G = G_1(1-c) + G_2c + Uc(1-c) + RT[c\ln c + (1-c)\ln(1-c)] \tag{1}$$

where G_1 and G_2 are the Gibbs potentials of 'pure components', c and $(1-c)$ are their molecular concentrations, $Uc(1-c)$ is the mixing energy of the system, and $R[c\ln c + (1-c)\ln(1-c)]$ is the configuration entropy of mixing.

Formally, expression (1) is completely analogous to that for the regular solutions of ordinary two-component systems, but it has an important feature. Equation (1) describes the properties of a system that is, in fact, a one-component system rather than a two-component one. The clusters of two kinds are pseudo-components because they may transform from into one another. Therefore, c is not an independent external parameter, but is an internal parameter that is adjusted under variable external parameters T and P so as to minimize the G-value. As a result, the T–P diagram has no two-phase region and includes only a line of two-phase equilibrium. With these features taken into account, it is reasonable to define the systems under consideration as pseudo-binary systems and both phases as pseudo-binary solutions.

It has been shown in [1] that the model of the pseudo-binary solutions is quite similar to the statistical model proposed by Strässler and Kittel for the two-level systems [2] in which the energy for excitation to the higher energy level, ε, is a linear function of the excitation, χ: $\varepsilon = \varepsilon_0 + \lambda\chi$. The present model is simply recast in terms of formal thermodynamics that are more obvious and convenient for description of the phase diagrams. All of the coefficients in expression (1) have a simple meaning. Concentration c corresponds to the degree of excitation, χ, in the statistical model [2], and the mixing energy is $U = \lambda/2$.

The model of the pseudo-binary solutions was first proposed in [3] for calculation of the stable $T-P$ diagram of Ce that includes the equilibrium line of two isomorphous phases terminating at the critical point. Also calculated were the changes of the volume jump and the transition heat along the equilibrium line, and the anomalies of the compressibility, as well as the nature of the minimum in the melting curve, were brought to light [4]. The calculated data were in excellent agreement with the experimental ones. At the same time, Rapoport [5] suggested a similar concept that he called a two-liquid model in order to explain maxima in the Rb and Cs melting curves. The expression for the Gibbs potential in this model was the same as in [3, 4] for cerium, the only difference being that the components were clusters rather than atoms. Aptekar [6] was the first to use the model of regular solutions of two types of cluster to calculate the metastable $T-P$ diagrams of germanium and silicon in the disordered (both liquid and amorphous) state. Ponyatovsky and Pozdnyakova [7] calculated the metastable $T-P$ diagrams of several III–V compounds. The same model was used to calculate the metastable $T-P$ diagram of disordered water with a second critical point [8]. The analytic expressions for the anomalies of the thermodynamic properties of water at atmospheric pressure were also derived [9].

For water, experimental data on the thermodynamic properties at atmospheric pressure and on the high-pressure phase transitions are more abundant than for other substances whose metastable phase diagrams have been calculated within the model of regular pseudo-binary solutions. In view of this, the applicability of the thermodynamic model is illustrated first for the example of water, and then we consider interesting consequences deduced for some other substances.

3. Water

The anomalous properties of water supercooled below the melting point have been the focus of research interest for a long time. Angell *et al* [10–13], who developed a method for supercooling water using emulsion media, have considerably extended the interval of water supercooling. Using this method, the thermal dependence of the main thermodynamic properties of water was accurately measured for temperatures as low as $-42\,^{\circ}$C. The thermal behaviour of the properties is similar to that of substances in the vicinity of the second-order phase transition or near the spinodal where a phase loses stability. There was long discussion on two feasible scenarios: continuous or discontinuous behaviour of the thermodynamic properties of water upon supercooling to low temperatures [14, 15].

Very important data for understanding the nature of anomalies in supercooled water have been obtained by Mishima *et al* [16–18] from high-pressure study of SSA of ice. In their pioneering work [16], they found that two different modifications of amorphous ice could be prepared, depending on the parameters of the thermobaric treatment, i.e. high-density amorphous ice (hda) and low-density amorphous ice (lda). The hda specific volume is $\sim$20 % less than that of lda, and the lda–hda transition is a reversible first-order phase transition [18]. In the present two-level model of water, the different energy states are groups of H_2O molecules that differ in short-range order. These groups of molecules are accepted here as clusters. The occurrence of two basic structural states of water with different types of short-range order is supported by the experimental data on the structure [19–21] as well as by molecular dynamical simulations [22–24].

The degree of excitation of the system, c, is defined as the proportion of H_2O molecules with the hda-like atomic configuration. The ground state, i.e. pure component 1, is attributed to the structural state corresponding to the lda phase at atmospheric pressure and low temperatures. The excited state, i.e. component 2, is the hda structural state in its stability region at high

pressures and low temperatures. The concentration-dependent part of the Gibbs potential is of the form

$$\Delta G(T, P, c) = G - G_1 = (\Delta E^0 - T\,\Delta S^0 + P\,\Delta V^0)c + Uc(1-c) + RT[c\ln c + (1-c)\ln(1-c)] \quad (2)$$

where $\Delta E^0 = E_2 - E_1$, $\Delta S^0 = S_2 - S_1$, and $\Delta V^0 = V_2 - V_1$.

Parameter c is determined by minimizing the Gibbs potential, $G(c)$:

$$\left.\frac{\partial G}{\partial c}\right|_{T,P} = (\Delta E^0 - T\,\Delta S^0 + P\,\Delta V^0) + U(1-2c) + RT\ln\frac{c}{1-c} = 0. \quad (3)$$

The first term in parentheses in equation (3) is zero at the phase equilibrium line; therefore the phase equilibrium temperature is expressed using equation (3) as

$$T_{eq} = \frac{U}{R}\frac{1-2c}{\ln\frac{1-c}{c}}. \quad (4)$$

Four quantities in equation (3), ΔE^0, ΔS^0, ΔV^0, and U, are accepted to be independent of T and P throughout the T–P region that we consider; thus, they constitute a set of model constants. To determine the Gibbs potential, it is sufficient to find the values of these four constants. The first estimate of the values is obtained directly from the experimental data.

The experimental value of the volume jump at the $lda \rightarrow hda$ transition is equal to -4 ± 0.2 cm^3 mol^{-1} at $T = 77$ K and $P = 0.55$ GPa [17]. The equilibrium pressure of this transition at $T = 77$ K is about 0.2 GPa [17]. We assume that the extension of the lda–hda equilibrium line to atmospheric pressure should intersect the temperature axis within an interval corresponding to probable extrema of the low-temperature anomalies of the thermodynamic properties, i.e. between 225 and 228 K [10, 11, 13]. Note that this extrapolation of the lda–hda equilibrium line brings the system into the region of the liquid state over $T = T_g(P)$. But there is no first-order phase transition at T_g; therefore the lda–hda equilibrium line and the spinodals as well as their first derivatives do not have a discontinuity at T_g. For the sake of universality, we do not distinguish between the liquid and amorphous states in the calculations of the phase diagrams below, and denote both states as disordered ones.

The slope of the lda–hda equilibrium line thus deduced and the volume jump give an approximate ΔS^0 value: $3.8 \leqslant \Delta S^0 \leqslant 5.4$ J mol^{-1} K^{-1}. A linear extrapolation of the equilibrium line to $T = 0$ K results in a transition pressure which should satisfy the relation $P(0) = \Delta E^0/\Delta V^0$. This gives an estimated value of $\Delta E^0 = 0.84$–1.26 kJ mol^{-1}. Such linear extrapolation is not correct in the physical sense in the limit of $T = 0$ K, because it does not take into account the third law of thermodynamics, but it can be used as a first approximation. To find the U-value, we use a relation that is valid for the regular pseudo-binary solutions at the critical point (see [9]):

$$T_{cr} = U/2R. \quad (5)$$

Accepting $T_{cr} \approxeq 228$ K as the first approximation, we obtain $U = 3.79$ kJ mol^{-1}.

Further fitting of the model constants to the available experimental data resulted in the following final values: $\Delta E^0 = 1.04$ kJ mol^{-1}, $\Delta S^0 = 4.23$ kJ mol^{-1} K^{-1}, $\Delta V^0 = -3.8$ cm^3 mol^{-1}, and $U = 3.83$ kJ mol^{-1}. These values were used in all further calculations.

3.1. The metastable T–P phase diagram of water

With the values of all four constants known, expression (1) for $G(c)$ allows us to calculate the equilibrium line between the ldd and hdd (low-density disordered and high-density disordered, respectively) phases, the boundaries of the thermodynamic stability (the spinodals), the

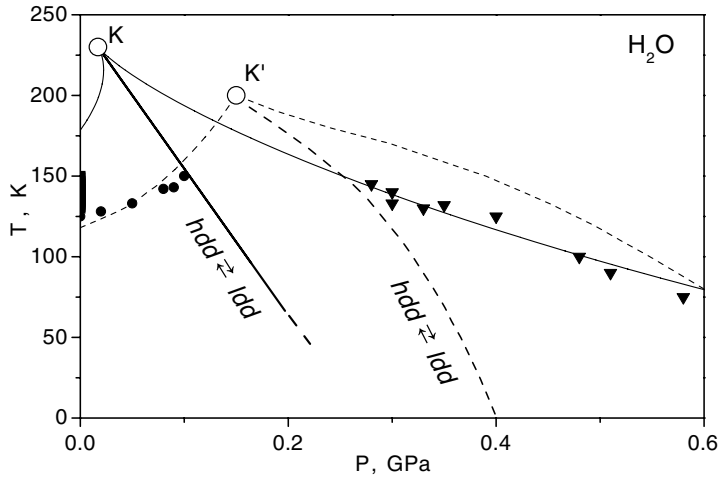

Figure 1. The metastable T–P phase diagrams of water calculated with the thermodynamic model [8, 9] (solid curves) and with the MDS method [22–24] (dashed curves). Also labelled are the critical points, K and K′, and the hdd–ldd equilibrium lines between the low-density and high-density disordered phases. Circles and triangles show the experimental data on the hdd → ldd and ldd → hdd transitions at P = constant [18], and the vertical bar is for the experimental data on the hdd → ldd transition at $P = 1$ atm [25].

coordinates of the critical point, as well as the anomalies of the thermodynamic properties near the critical point and the spinodals. Figure 1 presents the metastable T–P phase diagram of water. The thick solid curve shows the curve of equilibrium between two disordered phases. Its equation is

$$G_1(T, P) = G_2(T, P) \qquad \text{or} \qquad \Delta E^0 - T\,\Delta S^0 + P\,\Delta V^0 = 0. \tag{6}$$

Hence, the ldd–hdd equilibrium line in the present model is a straight line with a slope $\mathrm{d}T/\mathrm{d}P = \Delta V^0/\Delta S^0 = -900\ \mathrm{K\ GPa^{-1}}$.

The spinodals are plotted as thin solid curves. The equation for the spinodals is

$$\frac{\partial^2 G}{\partial c^2} = -2U + \frac{RT}{c(1-c)}. \tag{7}$$

$G(c)$ has two minima inside the region limited by the spinodals, and both phases may occur in this region. The deeper minimum corresponds to the more stable phase; the shallow one is for the phase of lower stability. K is the critical point with the coordinates $T_{cr} = 230$ K and $P_{cr} = 0.0173$ GPa.

There are also plotted experimental data for the ldd → hdd and hdd → ldd transitions from compressibility measurements [18] and neutron diffraction data for the ldd → hdd transition observed upon heating of the crystalline high-pressure phase at $P = 1$ atm [25]. All experimental data are inside the T–P region limited by the spinodals. The data on the ldd → hdd transition are close to the spinodal, though these data were not used at all for the determination of the model constants.

3.2. Anomalies of the thermodynamic properties at atmospheric pressure

The analytical expressions describing the anomalies of the thermodynamic properties of water as functions of T, P, c, ΔE^0, ΔS^0, ΔV^0, and U are readily obtained from the expression for

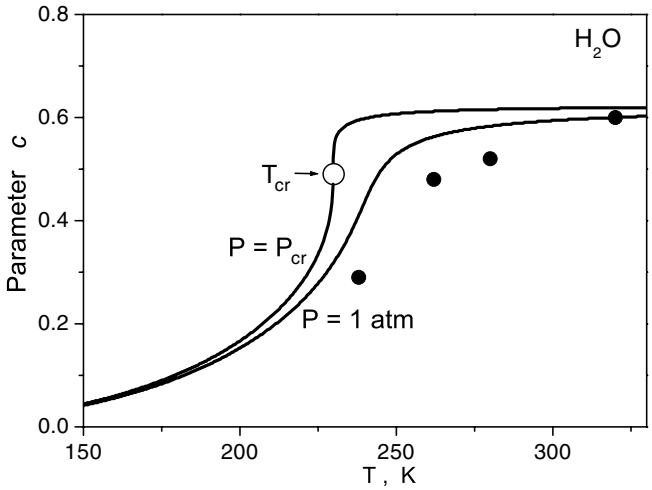

Figure 2. Parameter c: its dependence on temperature at $P = 1$ atm and $P = P_{cr}$ [9]. The curves are calculated with the thermodynamic model [8, 9]; the solid points are obtained from the structural data [20].

the Gibbs potential, equation (1). (An anomaly is defined as a deviation of some property from the normal behaviour, as usual.) So, the anomalous parts of the thermal expansion coefficient, α, the isothermal compressibility, γ_T, and the specific heat, C_P, are given as, respectively [9],

$$\Delta\alpha(T) = \frac{\Delta V^0}{V}\left(\frac{\partial c}{\partial T}\right)_P \tag{8}$$

$$\Delta\gamma_T(T) = \frac{\Delta V^0}{V}\left(\frac{\partial c}{\partial P}\right)_T \tag{9}$$

$$\Delta C_P(T) = (\Delta E^0 + P\,\Delta V^0 + U - 2cU)\left(\frac{\partial c}{\partial T}\right)_P \tag{10}$$

where

$$\left(\frac{\partial c}{\partial T}\right)_P = \frac{\Delta V^0}{2U - \frac{RT}{c(1-c)}} \tag{11}$$

$$\left(\frac{\partial c}{\partial P}\right)_T = \frac{R\ln\frac{c}{1-c} - \Delta S^0}{2U - \frac{RT}{c(1-c)}}. \tag{12}$$

The principal factor in each of equations (8)–(10) is represented by the c-derivative with respect to T or P. The behaviour of parameter c in the T–P plane should therefore be considered first.

Figure 2 shows the calculated $c(T)$ isobars for $P = 1$ atm and for $P = P_{cr}$. It is seen that the $c(T)$ isobar at $P = P_{cr}$ is very steep in a narrow interval of 200 K $< T <$ 235 K. When $T \to T_{cr}$, the c-derivative tends to infinity: $\partial c/\partial T \to \infty$. In contrast, parameter c approaches a value of 0.6 near $T = 240$ K and then changes negligibly on further heating. At atmospheric pressure the $c(T)$ dependence has no singularities, parameter c visibly changes up to $T = 300$ K, and the maximum value of $\partial c/\partial T$ is reached at $T = 235$ K, which is the temperature limit of supercooling achieved in the $C_P(T)$ measurements using the emulsion method [11].

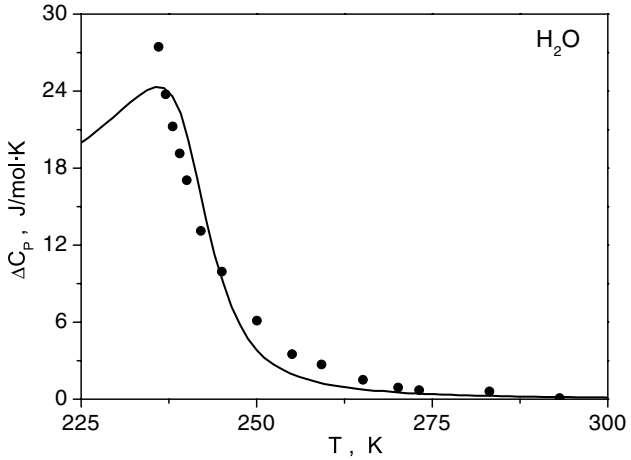

Figure 3. The anomaly of the H_2O specific heat at $P = 1$ atm. Points represent the experimental data [13], and the solid curve is a fit with the thermodynamic model [9].

Bellissent-Funel [20] has calculated the $c(T, P)$ parameter from the structural data at different temperatures and pressures. The full pair correlation function of water, $d_L(r, T, P)$, was presented as a superposition of the pair correlation functions of the low-density and high-density phases of water. The c-values calculated in [20] are also plotted in figure 2. A fairly good correlation between the two calculated results is obvious. Both the thermodynamic model and the calculation based on the experimental structural data result in the same value of parameter c near room temperature, $c = 0.6$. This can hardly be a mere coincidence, because the two approaches involved are independent.

The above consideration demonstrates that the concentration of high-density clusters, c, changes most drastically in the temperature interval of 210–250 K, just where the anomalies of the physical properties of supercooled water are strongest. Above $T = 300$ K, parameter $c(T)$ depends on temperature only weakly, its value being close to 0.6. The negligible thermal dependence of parameter c results in normal thermal dependence of properties of water above 300 K. Figures 3 and 4 represent the thermal dependences of the anomalies of water calculated from equations (8)–(12) together with the experimental data from [10–13]. The agreement between the calculated and experimental data is quite satisfactory.

Now we compare the metastable T–P phase diagram of water plotted in figure 1 with those obtained using the molecular dynamics simulation (MDS) method. The first successful calculation of the metastable T–P diagram was realized by Poole *et al* [22]. The metastable T–P diagram calculated by means of MDS [22] is plotted also in figure 1 (the dashed curves). It is seen that the two T–P diagrams are topographically similar, but there is a quantitative difference as regards the positions of the equilibrium line, the spinodals, and the coordinates of the critical point. It is essential for the critical point, in both diagrams, to be at a positive pressure value. This means that the anomalies of water correspond to the continuous scenario. Later, Tanaka published a T–P diagram also calculated using MDS [26], but with the coordinates of the critical point equal to $T_{cr} = 240$ K and $P_{cr} = -0.1$ GPa, which corresponds to a discontinuous thermal behaviour of the properties at atmospheric pressure.

A long discussion on continuous or discontinuous scenarios was completed by Mishima [27]. Mishima measured the melting curves of the crystalline high-pressure D_2O phases, ice III, IV, and V, in their metastability regions. To avoid transitions to the stable

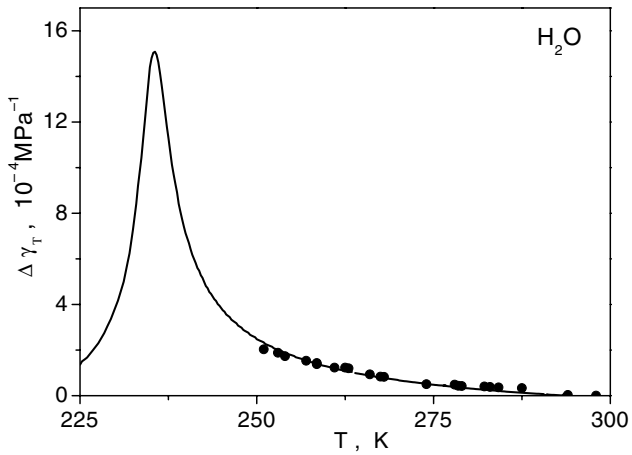

Figure 4. The calculated thermal dependence of the isothermal compressibility of water at $P = 0.01$ GPa (solid curve) [9] as compared to the experimental points [57].

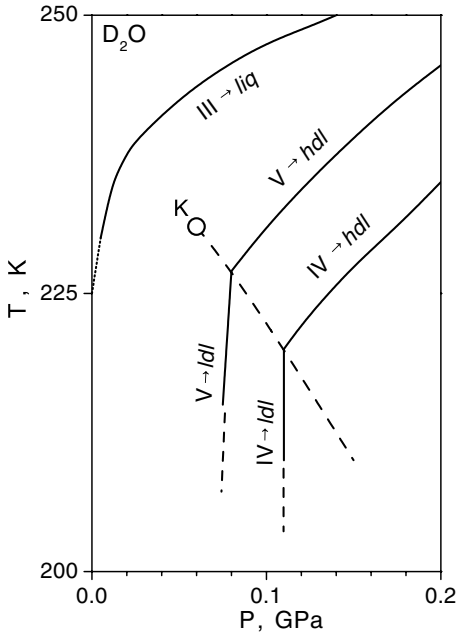

Figure 5. A schematic plot of the melting curves of the D_2O phases, ice III, IV, and V, measured on decompression (solid curves) [27]. The dashed line shows the presumed line of hdd–ldd equilibrium, and K is the critical point.

crystalline phases, the emulsion method was used. The melting points were fixed in decompression runs. Figure 5 presents a schematic plot of the experimental melting curves of ice III, IV, and V. A sharp break of the slope is observed in the melting curves for ice IV and V, whereas that of ice III is continuous and smooth to atmospheric pressure, demonstrating a distinctly supercritical behaviour. Mishima related the break points in the ice IV and V melting curves to the crossing of the phase equilibrium line between the low-density liquid

(ldl) and high-density liquid (hdl). So, these data give the position of the ldl–hdl equilibrium line and rough coordinates of the critical point that should be between the ice III and V melting curves. The estimated coordinates of the critical point are $T_{cr} = 230 \pm 5$ K and $P_{cr} = 500 \pm 200$ atm [27], which is in accord with the values calculated within the present thermodynamic model.

A general conclusion from the theoretical and experimental data discussed above is that the anomalous properties of supercooled water are a consequence of the occurrence of the second critical point at a positive pressure, $P > 1$ atm. Hence, these are supercritical anomalies.

4. Silicon, germanium and A_{III}–B_V compounds (GaSb, GaAs, and InSb)

The validity of the model of the pseudo-binary solutions for the analysis of the metastable T–P diagrams of semiconductors with the tetragonal structure is demonstrated by the experimental data on the behaviour of melts [28] and the SSA of these substances [29, 30], and supported by the theoretical interpretation of the structure of disordered Ge and Si [31, 32]. The discussion below concerns the thermodynamic aspects of the T–P diagrams including feasible liquid–liquid and amorphous–amorphous phase transitions.

Regel and Glazov [28] observed an anomalous increase of the viscosity and the electric resistivity of the liquid semiconducting elements Si and Ge and several A_{III}–B_V compounds when temperature approached the crystallization point. They explained the anomalies discovered in terms of the formation of tetrahedrally coordinated clusters whose concentration in the metallic melt increased with lowering temperature, and determined the thermal dependence of their concentration. These data gave a good experimental basis for calculation of the metastable T–P phase diagrams of the supercooled disordered states for Ge and Si [6] and for the A_{III}–B_V compounds [7] using the model of the pseudo-binary solutions. All metastable diagrams calculated for these semiconducting substances include a first-order transition line that terminates at the critical point in the range of negative pressures. The speculation on these substances is much simplified compared to that for water because:

(i) All of them have the only crystalline modification at atmospheric pressure, i.e. the semiconducting phase with tetrahedral coordination transforms to the more closely packed metallic phase under high pressure. The assumption of only two types of cluster in the melt coordinated according to these two polymorphous modifications seems rather uncontroversial therefore.
(ii) The stable T–P phase diagrams are studied in considerable detail.
(iii) The structure and the electric properties of the amorphous semiconducting films prepared using vapour deposition are known.
(iv) The SSA of the GaSb high-pressure phase, GaSb II, as well as the structure, the thermal stability, and the electric properties of the amorphous samples have been studied experimentally in detail [29, 30, 33].

In contrast to water, however, the melts of these semiconductors cannot be supercooled well below the melting point. Experimental data on the properties of supercooled metallic melts are therefore not available, which makes determination of the model constants, and hence the calculated metastable T–P diagrams, less reliable. The T–P diagrams are therefore calculated on a semiquantitative level. Nevertheless, the analysis of the diagrams obtained elucidates some features of the T–P behaviour of the disordered phases of the two-level systems. This is illustrated below for GaSb as a representative of the tetrahedrally coordinated substances.

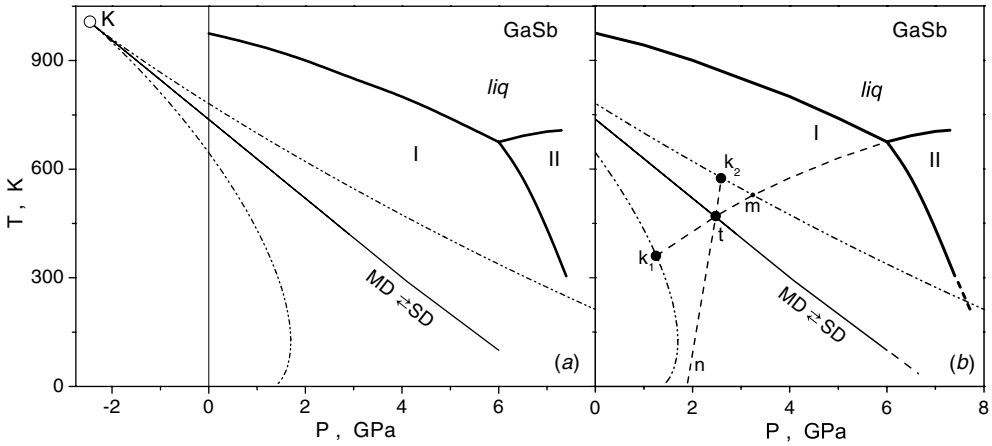

Figure 6. The stable and metastable $T-P$ phase diagrams of GaSb. Part (a) shows: the experimental lines of the stable phase equilibria (bold solid curves); the calculated line of metastable equilibrium between the metallic disordered and semiconducting disordered phases (thin solid curve); the calculated spinodals (dash–dotted curve); and the critical point, K [7]. Part (b) presents a schematic explanation of feasible equilibria between the stable and metastable phases: k_1tm is the extrapolation of the phase II melting curve limited by the pseudo-critical point k_1; the metastable II–SD phase equilibrium line, ntk_2, is limited by pseudo-critical point k_2; and t is the triple point of the metastable equilibrium, SD–MD–II.

The stable and metastable GaSb phase diagrams are presented in figure 6(a). The metastable equilibria in disordered GaSb are calculated using equation (1) with the following model constants: $\Delta E^0 = 21\,\mathrm{kJ\,mol^{-1}}$, $\Delta S^0 = 28.4\,\mathrm{kJ\,mol^{-1}\,K^{-1}}$, $\Delta V^0 = -3.06\,\mathrm{cm^3\,mol^{-1}}$, and $U = 16.8\,\mathrm{kJ\,mol^{-1}}$ [7].

The analysis of the experimental data on SSA raises several questions. There are many works where pressure-induced SSA of crystals is treated as a result of crossing of the melting curve of the given crystalline phase extrapolated to the metastability region. This idea is called the cold-melting hypothesis. If this hypothesis is followed, quenched phase GaSb II should transform to the metallic disordered phase when heated above the point of intersection of its melting curve with the T-axis. Under the assumption of cold melting, this transition appears to be endothermic, like in other cases of melting. Upon further heating, the metallic glass would transform to another phase with a lower Gibbs potential: either to the stable semiconducting crystalline phase I or to the metastable semiconducting disordered phase. Quenching from the melt at a high rate also would result in metallic glass. Metallic glass, however, has never been obtained using the various techniques of high-rate quenching from the metallic melt. When metastable crystalline phase II is heated at atmospheric pressure, it undergoes a transition directly to the semiconducting amorphous phase with tetrahedral coordination. Neither amorphous metallic phase was observed even as an intermediate stage of SSA. The GaSb II $\rightarrow$ amorphous phase transition is concomitant with heat evolution rather than absorption as in the case of melting. What is the nature of these phenomena, contradicting the cold-melting hypothesis? The metastable $T-P$ diagram calculated on the basis of the thermodynamic model explains this behaviour of GaSb.

Consider the GaSb phase diagram presented in figure 6(a). When quenched at $P =$ 1 atm, the melt has to cross the line of the MD $\rightarrow$ SD (metallic disordered–semiconducting disordered) phase equilibrium. The MD $\rightarrow$ SD transition that would occur at a temperature no less than the boundary of the stability region for the MD phase (lower spinodal) would

result in considerable heat evolution, and, hence, a delay in cooling leading to crystallization. This is why the MD state cannot be retained in high-rate quenching of the GaSb melts. The MD state is thermodynamically unstable at atmospheric pressure and temperatures below the MD spinodal. SSA of the quenched GaSb II phase on heating occurs below the MD spinodal. This is why the crystal II $\rightarrow$ SD transition takes place.

Now we discuss whether there is a correlation between the extrapolation of the melting curve to $P = 1$ atm and amorphization of the high-pressure phase on heating—in other words, whether the hypothesis of cold melting is applicable for explaining SSA of GaSb. For this purpose, all possible phase equilibria due to extrapolation of the phase II melting curve to the metastable region are considered in figure 6(b). Only one metastable equilibrium, II–MD, is possible in the interval between the 'liq–I–II' triple point and point m. Both metastable phases, SD and MD, are feasible in interval mt of the extended melting curve, but $G_{MD} < G_{SD}$ here—that is, the MD phase stays more stable than the SD one. The relation of the Gibbs potential is opposite in the interval tk_1, $G_{SD} < G_{MD}$, and the SD phase becomes more stable than the MD one. Finally, point k_1 is a permissible limit for extrapolation of the II $\rightarrow$ MD melting curve. The Gibbs potential has only one minimum in the region to the left of point k_1. This minimum corresponds to the SD phase whereas MD is thermodynamically totally unstable and therefore is no longer a phase. Because the melting curve is a line of either stable or metastable equilibrium between two phases, the melting curve in question terminates at the point where one of the phases stops existing. Therefore, further extrapolation of the melting curve has no physical sense. There is a clear-cut distinction between point k_1 and classical critical points ending the lines of the liquid–vapour, 'am I–am II', or fcc Ce I–fcc Ce II isomorphous phase equilibria. Approaching a classical critical point, two phases become closer in their properties, and both become unstable at the point. In contrast, k_1 is a point where only one of the phases, the disordered one, becomes unstable, and the difference between the phases remains intact. This special point was therefore defined in [34] as the pseudo-critical point.

This example shows that there are some substances with phase diagrams shaped similarly to the T–P diagram of water, but extrapolation of the melting curves of their high-pressure phases to low temperatures and zero pressure is not possible. The hypothesis of cold melting is therefore not universal and applicable to all substances with no exceptions.

There is another interesting feature of the GaSb metastable diagram. Point t is the intersection point of two equilibrium lines, the MD–GaSb–II melting curve and the MD–SD equilibrium line between two disordered phases. According to the phase rule, t should be the triple point of the MD–SD–II equilibrium, and the third line, the II–SD equilibrium line, should also pass through this point. This line is an analogue of the MD–II melting curve, the only difference being that the crystalline metallic phase crossing this line undergoes a transition to the semiconducting disordered phase, SD, liquid above T_g and amorphous below T_g. This line is shown in figure 6(b) as ntk_2. Its slope with respect to the pressure axis depends on the value and the sign of the entropy jump, the latter being larger, less than, or equal to zero. Hence, the line of the II–SD equilibrium, ntk_2, may have either positive or negative slope, or it can be vertical. Intersection of the metastable II–SD equilibrium line with the boundary of thermodynamic stability of the SD phase (top spinodal) is a new pseudo-critical point, k_2. The II–SD equilibrium line terminates at the point k_2. So, the triple point t is the intersection point of three metastable equilibrium lines, one of them terminating at a classical critical point and the other two terminating at the pseudo-critical points.

To conclude, the analysis of the superposed stable and metastable diagrams gives a number of topological elements that are absent in each diagram separately. At first sight, the topological features of the metastable T–P phase diagrams as well as the pseudo-critical points appear to be only of academic interest and to have no direct relation to the experimental data on the

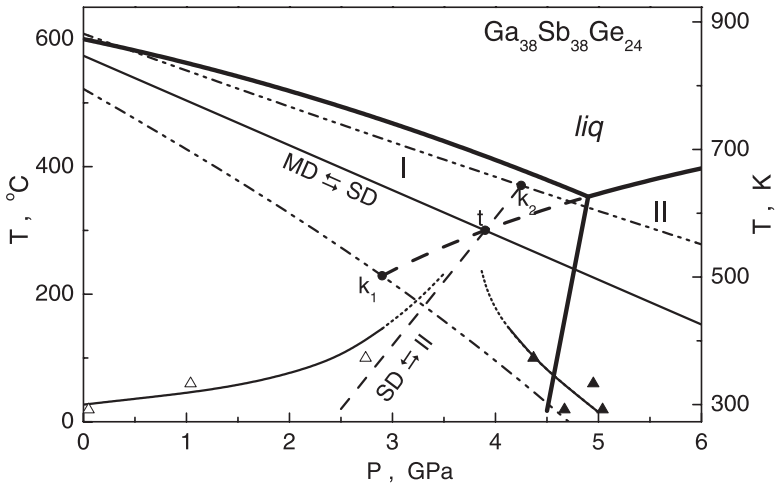

Figure 7. The stable and metastable T–P phase diagrams of $Ga_{38}Sb_{38}Ge_{24}$ [35, 36]. Shown are the lines of the stable equilibria (bold solid curves), the extrapolation of the phase II melting curve (bold dashed curve), the calculated line of the metastable equilibrium between the metallic and semiconducting disordered phases (thin solid curve), the calculated spinodals (dash–dotted curves). Thin solid lines below 150 °C and their extensions (dotted) to higher temperatures represent the kinetic curves of the II → SD and SD → II phase transitions, and the thin dashed line is the metastable II–SD phase equilibrium line. Pseudo-critical points are designated as k_1 and k_2, and t is the triple point of the SD–MD–II metastable equilibrium. The experimental points of the II → SD and SD → II phase transitions are plotted as open and solid triangles.

phase transitions in the systems under consideration. There are, however, several examples where the thermodynamic concept of the metastable T–P phase diagrams developed here is useful for analysis of the experimental data obtained in the stability regions of liquid as well as amorphous phases.

(1) Antonov *et al* [35, 36] observed reversible SSA of the metallic phase resulting in the semiconducting amorphous phase (II–SD) on compression and decompression of the $Ga_{38}Sb_{38}Ge_{24}$ alloy (see figure 7). The transformation has a large hysteresis increasing with lowering temperature. The calculated line of the II–SD metastable equilibrium is between the kinetic curve of the direct and reverse transitions, as it should be. Therefore, the II–SD equilibrium line in figure 7 corresponds to line ntk_2 in figure 6(b). Note that the kinetic curve of the transformation oversteps the graphic extrapolation of the MD–II melting curve around $T = 40\,°C$.

(2) The other example is given by Mishima [27] in the above-mentioned measurements of the metastable melting curves of the D_2O crystalline phases, ice IV and V (see figure 5). The melting curves of ice IV and ice V have distinct breaks of slope. The low-temperature parts of the ice IV and V melting curves are close to vertical. The top part of each curve corresponds to the crystal hdl equilibrium, and the low-temperature part corresponds to the crystal ldl equilibrium. The low-temperature parts are analogues of line ntk_2 in figure 6(b) and have different slopes because different crystalline phases, IV and V, are in equilibrium with the same liquid phase.

(3) In both cases above, the curves for the transition between the crystalline high-pressure phase and the low-pressure disordered phase are analogous from the formal thermodynamic point of view within the present model. Note, however, an important

difference between the experimental conditions in the measurements on D_2O and on the Ga–Sb–Ge alloy. The difference is that the experiments on D_2O [27] were carried out at $T > 200$ K, i.e. above the glass transition temperature, T_g ($T_g \approx 150$ K for water), whereas the $Ga_{38}Sb_{38}Ge_{24}$ alloy in [35, 36] was studied below T_g. This resulted in a crucial kinetic difference of the disordering process. Disordering of the high-pressure D_2O phases takes place immediately upon crossing each equilibrium line, IV ldl or V ldl, as at normal melting of the stable phase. In contrast, amorphization of the $Ga_{38}Sb_{38}Ge_{24}$ alloy is characterized by a hysteresis increasing at lower temperatures, as at the crystal–crystal phase transitions. This example shows also that a correlation between the glass transition temperature and the metastable phase diagram is also very important for interpretation of the available experimental data on the metastable transitions.

(4) The nature of the exothermal heat effect due to transition of the crystalline phases quenched under pressure to the semiconducting amorphous state observed in the Ga–Sb and Ga–Sb–Ge systems at $P = 1$ atm [29, 35] is now cleared up. Amorphization of these substances takes place at a point separated from the II–SD equilibrium curve by the value of P_{eq}. The heat effect of SSA at atmospheric pressure therefore consists of two terms: $\Delta H = \Delta H_{eq} + P_{eq}\,\Delta V$ where $\Delta H_{eq} < 0$. But the absolute value of ΔH_{eq} is less than that of the $P_{eq}\,\Delta V$ term. The sign of the heat effect is therefore determined by the $P_{eq}\,\Delta V$ term corresponding to the exothermal effect. For example, $P_{eq}\,\Delta V \approx +7.4$ kJ mol^{-1} for GaSb, and the experimental heat effect due to amorphization is $\Delta H = +3.5$ kJ mol^{-1} [29]; hence, $\Delta H_{eq} \approx -3.9$ kJ mol^{-1} at equilibrium pressure.

5. Carbon

Carbon is another interesting and very important substance for which calculation of the metastable phase diagram was attempted, involving a feasible phase transition in the liquid state. Figure 8 shows the melting curves of carbon presented in [37–39]. There are great differences, qualitative and quantitative, among the reported melting curves. Line 1 is a curve with a flat maximum whereas lines 2 and 3 exhibit a distinct break of slope. The pressure values corresponding to the maximum and the breaks of slope are approximately the same, 5–6 GPa, but the melting temperatures differ by about 400 K both at maximum and on extrapolation to atmospheric pressure. Curve 2 is plotted according to the latest experimental data, and Bundy *et al* [37] considered it to be the most reliable. Later research, however, resulted in a shift of the graphite–liquid–vapour triple point by 1000 K, from 4000 to 5000 K [37, 40]. On the other hand, melting curves 2 and 3 extrapolated to $P = 1$ atm give ≈4600 K rather than 5000 K. This comparison shows that the actual shape of the melting curve has not become clear so far. The discrepancy in the data is caused by the great difficulty of experimental determination of the melting curve of so refractory a material as carbon.

The shapes of the melting curves in figure 8 as well as the available experimental and theoretical data on carbon [38, 39, 41, 42] suggest that liquid and amorphous carbon should undergo a transition from the graphite-like phase (coordination $n = 3$) to the diamond-like amorphous phase (coordination $n = 4$) under high pressure. The presumed metastable diagram for the disordered phases—in particular, the position of its critical point with respect to the stable T–P diagram—is strongly correlated with the shape of the stable melting curve. A flat maximum is indicative of the position of the critical point below the melting curve, whereas the broken curve suggests that the critical point is above the melting curve. So, previous calculations of the metastable diagrams resulted in different conclusions.

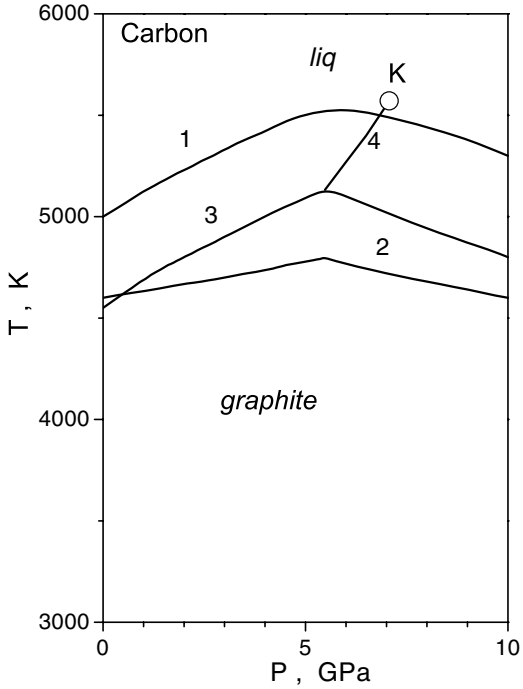

Figure 8. The high-temperature part of the stable T–P phase diagram of carbon. Plotted are the experimental melting curves from [37] (curve 1), from [39] (curve 2), and from [38] (curve 3), and the 'liq I–liq II' equilibrium line (curve 4) terminating at critical point K [38].

Korsunskaya *et al* [43] used the melting curve with a flat maximum suggested by Bundy in 1963 [44] in their calculation within the model of pseudo-binary solutions. They obtained a vertical line of 'am I–am II' equilibrium terminating at the critical point with the coordinates $T_{cr} = 3770$ K and $P_{cr} = 6.5$ GPa. Van Thiel and Ree [38] analysed the experimental and theoretical data on the properties of graphite, diamond, and the carbon melt available in 1993 and calculated a part of the T–P diagram within the model of two liquids. The calculated 'liq I–liq II' equilibrium line is presented in figure 8 as curve 4 with critical point K. The expression for the Gibbs potential corresponds to equation (1) for regular solutions, but for the mixing energy represented in the form

$$A_s(T, P, c) = RT\left[\frac{A_{S,0}}{1 + (P/P_0)^{3/2}}\right]c(1 - c) \tag{13}$$

where $A_{S,0}$ and P_0 are constants. The metastable equilibrium line obtained by van Thiel and Ree is, to a first approximation, a straight line between the graphite–diamond–liquid triple point at $T_{tr} = 5135$ K and $P_{tr} = 5.61$ GPa and the critical point at $T_{cr} = 5520$ K and $P_{cr} = 7.05$ GPa. The slope of the 'liq I–liq II' equilibrium line is $\mathrm{d}T/\mathrm{d}P = 270$ K GPa^{-1}.

The data calculated in [38] involve two ambiguities. There was no attempt to extend the 'liq I–liq II' equilibrium line to the region of the metastable equilibrium between two disordered phases below the triple point. Such extrapolation of the calculated equilibrium line to $P = 1$ atm gives the metastable equilibrium temperature of $T \approx 3700$ K. That is, the calculated data suggest that the diamond glass and the diamond liquid at atmospheric pressure are thermodynamically more stable than the graphite-like phases up to very high temperatures,

which contradicts the experimental data. It is well known that ordinary carbon glass produced at atmospheric pressure has a graphite-like atomic structure that stays stable on heating to high temperatures. Further, the mixing energy in equation (13) is a linear function of temperature (unless equation (13) is misprinted in [38]). This means that the mixing energy tends to zero when $T \to 0$, and the regular solution becomes an ideal solution with complete mutual solubility of the pseudo-components. This is extremely unusual. Usually, mutual solubility of the components in liquid and solid solutions decreases with lowered temperature and tends to zero when $T \to 0$ due to the decreasing negative contribution from the mixing entropy to the Gibbs potential. It is also unfortunate that van Thiel and Ree have not plotted the spinodals in their T–P diagram, because the positions of the stability boundaries of the disordered phases are important for evaluation of the T–P conditions in the experimental study of the phase transitions between the amorphous phases. For these reasons, the phase diagram reported in [38] does not seem very reliable.

So, the experimental data available at present are not sufficient for an accurate calculation of the metastable diagram of carbon. In spite of their uncertainty, below we attempt to compile the available experimental data and to use the thermodynamic model in order to suggest a realistic version of the metastable diagram. The latest data on the coordinates of the graphite–liquid–vapour triple point [40] indicate that the melting curve should be extrapolated to about 5000 K at $P = 1$ atm. Therefore, we accept curve 3 as the most reliable and shift it upwards by 400 K. Now the point of the break in curve 3 is between the maximum in curve 1 and the break point in curve 2, differing from them by about 50 K at the same pressure of 5.5 GPa. The 'liq I–liq II' equilibrium line (graphite-like liquid–diamond-like liquid) should pass through the break point at a much larger slope than line 4 in figure 8 and terminate at the critical point. A negative slope of this line is unlikely—for instance, from comparison with the equilibrium line between the graphite and diamond crystalline phases. Suppose the extreme case, a vertical 'liq I–liq II' line as in [43], and $T_{cr} = 5500$ K, which is close to the value presented in [38]. Depending on the preparation technique, the density of graphite-like amorphous carbon (carbon glass) ranges between 1.5 and 2.0 g cm^{-3}, and that of diamond-like amorphous carbon (diamond glass) is between 2.7 and 3.4 g cm^{-3}. The diamond-like amorphous carbon with the density of $\rho = 2.99$ g cm^{-3} was obtained from fullerene using shock-wave compression and the rapid-quenching technique [45, 46]. Diamond-like amorphous carbon with the density of 2.7–3.42 g cm^{-3} was also obtained by detonation of a mixture of an explosive with graphite [47]. We accept some average value for the model constant, $\Delta V^0 = -2.4$ cm^3 mol^{-1}. It is essential that this value affects only the positions of the spinodals in the T–P diagram, because the equilibrium line was accepted as being vertical. Other model constants are determined as $U = 2RT_{cr} = 45.9$ kJ mol^{-1}, $\Delta E^0 = P\,\Delta V^0 = 12.9$ kJ mol^{-1}, and $\Delta S^0 = 0$ kJ mol^{-1} K^{-1}. The metastable T–P diagram of carbon calculated using the model of pseudo-binary solutions is plotted in figure 9 together with the melting curve and the graphite–diamond equilibrium line.

The mutual disposition of the lines of stable and metastable equilibria in carbon suggests some assumptions on feasible transformations in the graphite-like disordered phase subjected to thermobaric treatment under various conditions. In the region of the thermodynamic stability of graphite and $T > T_g$, carbon glass should rapidly crystallize to graphite. In the stability region of diamond, the following transformations are possible:

(1) Carbon glass should crystallize to diamond at $T > T_g$. According to the empirical Kauzmann rule, $T_g \approx \frac{2}{3}T_m$ where T_m is the melting temperature. Following this rule, $T_g \approx 3000$ K for carbon. Note that the transition of the carbon glass to the labile state with high diffusion mobility of the atoms, as if it were 'melting', takes place at about

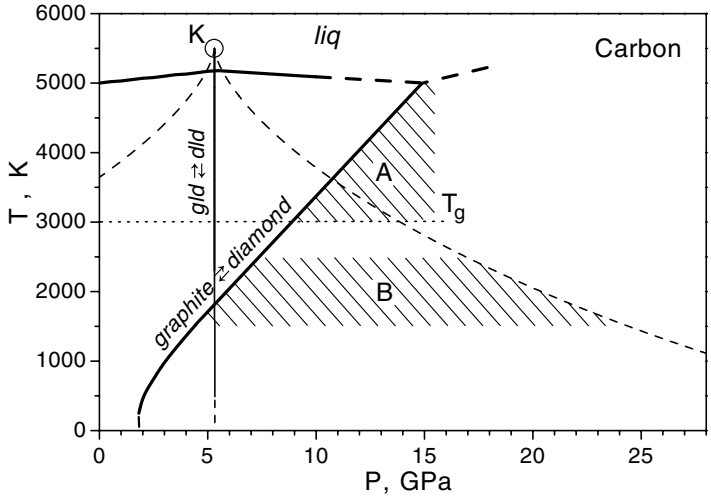

Figure 9. The presumed stable and metastable T–P phase diagram of carbon. The equilibrium graphite–diamond curve [37] and the melting curve are plotted as bold solid curves, the thin solid curve represents the metastable equilibrium between the graphite-like and diamond-like disordered phases ('gld' and 'dld', respectively), and the dashed curves are for the spinodals. The dotted line indicates the probable value of the glass transition temperature, T_g.

2000 K below the melting temperature of graphite. This facilitates synthesis of diamond from carbon glass, compared to graphite as the initial state, in hatched region A in figure 9.

(2) When $T < T_g$, carbon glass is expected to transform to different products. As temperature is lowered, the transformation product may wander from the equilibrium state, and formation of fine-grained diamond, nanocrystalline diamond, a mixture of nanocrystalline diamond and diamond-like amorphous glass, or 100% diamond-like amorphous product is anticipated. The assumed region of these transformations is shown as hatched region B in figure 9.

There is, however, a low-temperature limit below which the time of equilibration to the metastable state—that is, the time of relaxation to the corresponding local minimum of G—exceeds the characteristic experimental time. The thermodynamic models are no longer applicable in this T–P region (below hatched region B in figure 9). But carbon glass has low density; therefore it can become completely unstable on further compression. In this case, carbon glass is expected to transform to some intermediate disordered or crystalline states. Goncharov [48] observed an effect of this kind for nanocrystalline graphite and lda carbon compressed to 35 GPa at ambient temperature. The samples became transparent and disordered, though the Raman spectrum showed no hint of the diamond Raman band.

There have been many experiments on carbon in the form of graphite or fullerenes and subjected to high-pressure treatment at elevated temperatures (see [37, 45–47, 49]). It is surprising, however, that the transitions between graphite-like glass and diamond-like glass have been studied least. The experimental conditions corresponding to hatched region B are accessible to contemporary multi-anvil apparatuses. The diamond-like amorphous state and its composites with nanocrystalline diamond can be obtained in the form of bulk samples. These bulk samples are expected to have useful mechanical properties, because they should be superhard and should have no cleavage planes.

6. Conclusions

It follows from the above consideration that the behaviour of a substance in the $T-P$ plane is strongly dependent on the constitution of its melt. If the melt of the substance consists of two or more kinds of cluster markedly different in structure, internal energy, and specific volume, the substance is expected to show anomalous thermal and pressure dependences of its properties. Some features of such two-level systems represented by substances most studied currently are analysed here on the basis of a simple thermodynamic model of pseudo-binary regular solutions.

There are certainly many substances for which this model would be a rough approximation, inadequate for quantitative calculation of the metastable diagram and the anomalous properties of the liquid and amorphous phases. In some cases, taking into account more than two cluster types, a thermal and pressure dependence of the model constants, or some other model modification will be necessary for an accurate fit to the data. Further improvement can be achieved by the use of more sophisticated thermodynamic models of the multicomponent irregular solutions. Such models have already been successful when applied to multicomponent systems in metallurgy and mineralogy.

We can state, however, that the sophisticated models will retain the main features of the multilevel systems illustrated here using the examples of simple substances considered as two-level systems. That is, the metastable phase diagrams should include the first-order transition lines, the critical (pseudo-critical) points, and the resulting anomalies of the properties. The changes are expected at the quantitative level only—in particular, two or more phase equilibrium lines with critical points may occur in the $T-P$ diagrams of the multilevel systems representing the disordered state. Such an example has already been reported, e.g., for amorphous SiO_2 where two phase transitions, quartz-like $\rightarrow$ coesite-like and coesite-like $\rightarrow$ stishovite-like, were concluded to be occurring on the basis of the experimental data [50]. Two first-order transition lines above the melting curve are assumed for liquid S, Te, and P [51–54].

It is more crucial that a correct interpretation of the experimental data and prediction of unexplored phenomena in the multilevel systems requires knowledge of the superposition of the lines of stable and metastable equilibria. So, it is necessary to know both the stable and the metastable $T-P$ diagrams. There are two ways to calculate the metastable $T-P$ diagrams of the disordered substances considered so far: the MDS technique and thermodynamic modelling. There is no doubt that MDS is a more powerful method because it provides one with information both on the atomic structure and on the macroscopic properties of the subject of study. But the thermodynamic approach has its own advantages, such as clarity, simplicity, and deducibility of the analytic expressions describing all elements of the phase diagram and the anomalies of the thermodynamic properties in the vicinity of the critical point and the spinodals.

The number of two-level and multilevel systems is very large. These are numerous substances for which SSA was observed due to thermobaric treatment [55]. There are many binary systems with distinctly anomalous concentration dependences of the thermodynamic properties in the melt at atmospheric pressure. For the latter, Sommer proposed a thermodynamic model of solutions with so-called associates [56]. Associates in the Sommer model are just the same as clusters of a fixed stoichiometric composition and structure in the environment of the metallic melt. The model itself is based on chemical thermodynamics and uses the mass action law commonly applied in the description of chemical reactions. Substances of both named groups are representatives of multilevel systems.

In spite of a long previous history, activity in plotting the metastable $T-P$ phase diagrams of disordered substances is still at its initial stage. The most promising subjects for this activity

at present are elemental S, Se, Te, P, and I as well as the SiO_2 and GeO_2 compounds, for which some experimental and theoretical data are already available [51–54].

References

[1] Aptekar I L and Ponyatovsky E G 1968 *Phys. Met. Metallogr.* **25** 10
[2] Strässler S and Kittel C 1965 *Phys. Rev.* A **139** 758
[3] Aptekar I L and Ponyatovsky E G 1967 *Dokl. Akad. Nauk* **173** 851 (in Russian)
[4] Aptekar I L and Ponyatovsky E G 1968 *Phys. Met. Metallogr.* **25** 93
[5] Rapoport E 1967 *J. Chem. Phys.* **46** 2892
[6] Aptekar L I 1979 *Sov. Phys.–Dokl.* **24** 993
[7] Ponyatovsky E G and Pozdnyakova T A 1995 *J. Non-Cryst. Solids* **188** 153
[8] Ponyatovsky E G, Sinitsyn V V and Pozdnyakova T A 1994 *JETP Lett.* **60** 360
[9] Ponyatovsky E G, Sinitsyn V V and Pozdnyakova T A 1998 *J. Chem. Phys.* **109** 2413
[10] Rassmussen D H, MacKenzie A P, Tucker J C and Angell C A 1973 *Science* **181** 342
[11] Oguni M and Angell C A 1980 *J. Chem. Phys.* **73** 1948
[12] Angell C A, Oguni M and Sichina W J 1982 *J. Chem. Phys.* **86** 998
[13] Oguni M and Angell C A 1983 *J. Chem. Phys.* **78** 7334
[14] Angell C A 1982 *Water: a Comprehensive Treatise* vol 7, ed F Frank (New York: Plenum) p 1
[15] Speedy R J 1982 *J. Chem. Phys.* **86** 3002
[16] Mishima O, Calvert L D and Whalley E 1984 *Nature* **310** 393
[17] Mishima O, Calvert L D and Whalley E 1985 *Nature* **314** 76
[18] Mishima O 1994 *J. Chem. Phys.* **100** 5910
[19] Bellissent-Funel M-C, Teixeira J and Bosio L 1987 *J. Chem. Phys.* **87** 2231
[20] Bellissent-Funel M-C 1998 *Europhys. Lett.* **42** 161
[21] Bellissent-Funel M-C and Bosio L 1995 *J. Chem. Phys.* **102** 3727
[22] Poole P H, Sciortino F, Essmann U and Stanley H E 1992 *Nature* **360** 324
[23] Poole P H, Sciortino F, Essmann U and Stanley H E 1993 *Phys. Rev.* E **48** 4605
[24] Stanley H E, Angell C A, Essmann U, Hemmati M, Poole P H and Sciortino F 1994 *Physica* A **205** 122
[25] Balagurov A M, Barkalov O I, Kolesnikov A I, Mironova G M and Ponyatovsky E G 1991 *JETP Lett.* **53** 30
[26] Tanaka H 1996 *Nature* **380** 328
[27] Mishima O 2000 *Phys. Rev. Lett.* **85** 334
[28] Regel A R and Glazov V M 1983 *Sov. Phys.–Semicond.* **17** 1105
[29] Ponyatovsky E G and Barkalov O I 1996 *Phys. Status Solidi* b **198** 491
[30] Calvo-Dahlborg M, Dahlborg U, Barkalov O I, Kolesnikov A I, Ponyatovsky E G and Hannon A C 1999 *J. Non-Cryst. Solids* **244** 250
[31] Kresse G and Hafner J 1993 *Phys. Rev.* B **49** 14264
[32] Angell C A, Krishnan Sh, Felten J J and Price D L 1998 *J. Phys.: Condens. Matter* **10** 73
[33] Antonov V E, Barkalov O I and Kolyubakin A I 1996 *Phys. Status Solidi* b **198** 497
[34] Ponyatovsky E G 1997 *JETP Lett.* **66** 281
[35] Antonov V E, Barkalov O I, Ponyatovsky E G and Zavolovich S A 1997 *High Pressure Res.* **15** 201
[36] Antonov V E, Barkalov O I, Fedotov V K, Harkunov A I and Ponyatovsky E G 2002 *J. Phys.: Condens. Matter* **14** 1
[37] Bundy F P, Bassett W A, Weathers M S, Hemley R J, Mao H K and Goncharov A F 1996 *Carbon* **34** 141
[38] van Thiel M and Ree F H 1993 *Phys. Rev.* B **48** 3591
[39] Togaya M 1997 *Phys. Rev. Lett.* **79** 2474
[40] Baitin A V, Lebedev A A, Romanenko S V, Senchenko V M and Scheindlin M A 1990 *High Temp.–High Pressures* **22** 157
[41] Morris J R, Wang C Z and Ho K M 1995 *Phys. Rev.* B **52** 4138
[42] Fried L E and Howard W M 2000 *Phys. Rev.* B **61** 8734
[43] Korsunskaya I A, Kamanetskaya D S and Aptekar I L 1972 *Phys. Met. Metallogr.* **34** 39
[44] Bundy F P 1963 *J. Chem. Phys.* **38** 618
[45] Hirai H and Kondo K 1991 *Science* **253** 772
[46] Hirai H, Tariba Y, Kondo K, Oikawa T and Ishizawa N 1995 *Phys. Rev.* B **52** 6162
[47] Breusov O N, Abrosimova G A, Ananiin A V, Aronin A S, Drobyshev V N, Tatsii V F and Ponyatovsky E G 1996 *High Pressure Res.* **15** 191
[48] Goncharov A F 1990 *Zh. Eksp. Teor. Fiz.* **98** 1824 (in Russian)

[49] Sundqvist B 1999 *Adv. Phys.* **48** 1
[50] Elkin F S, Brazhkin V V, Khvostancev L G, Ziok O B and Lyapin A G 2002 *JETP Lett.* **75** 413
[51] Brazhkin V V, Popova S V and Voloshin R N 1997 *High Pressure Res.* **15** 267
[52] Katayama Y, Mizutani T, Utsumi W, Shimomura O, Yamakata M and Funakoshi K 2000 *Nature* **403** 170
[53] Grima P, Polian A, Gauthier M, Itie J P, Mezouar M, Weill G, Besson J M, Mäuserman D and Hanfland H 1995 *J. Phys. Chem. Solids* **56** 525
[54] Chrichton W A, Mezouar M, Grande T, Stolen S and Crzechnik A 2001 *Nature* **414** 622
[55] Sharma S M and Sikka S K 1996 *Prog. Mater. Sci.* **40** 1
[56] Sommer F 1982 *Z. Metallk.* **73** 77
[57] Kano H and Angell C A 1979 *J. Chem. Phys.* **70** 4008